

Taylor Cylinder and Convection in a Spherical Shell

M. Yu. Reshetnyak

Institute of Physics of the Earth, Russian Academy of Sciences, Bol'shaya Gruzinskaya ul. 10, Moscow, 123995 Russia
e-mail: m.reshetnyak@gmail.com

Received July 1, 2009; in final form, September 30, 2009

Abstract—The successive development of thermal convection in a rotating spherical shell heated from below has been studied. It has been indicated that the convection properties strongly differ within and outside a Taylor cylinder. The distributions of the kinetic energy, helicity, temperature, and differential rotation in these regions are presented. The consequences for the geodynamo theory and interpretation of geomagnetic observations are considered.

DOI: 10.1134/S0016793210020143

1. INTRODUCTION

The spherical geometry is typical of many astrophysical objects including stars and planets. This phenomenon is related to the predominance of centrally symmetrical gravitational force during the formation and further evolution of these objects. This property remains also true for convection (if originates) in certain regions of these objects. However, for a number of objects (mostly planets), convection in the cores, atmosphere, and ocean is defined by spherically symmetrical gravitational forces (as before) and by a rapid daily rotation, which results in a new type of symmetry—axial symmetry: when the axis of symmetry coincides with that of rotation. Convection can change from classical three-dimensional convection (daily rotation of an object is insignificant) into the state close to two-dimensional convection (rapid rotation). The latter state (the so-called geostrophic state [Pedlosky, 1987]) is caused by the fact that the Coriolis force twists any flow in the direction perpendicular to the axis of rotation, remaining fields parallel to the axis unchanged. Doing no work (force is perpendicular to velocity), the Coriolis force substantially affects the energy redistribution in the physical [Chandrasekhar, 1981] and wave [Reshetnyak and Hejda, 2008] spaces. Much attention is paid to the problems of convection in the works on the planet's and Earth's dynamo, where it is possible to consider only the Boussinesq model with heating from below [Jones, 2000] in a first approximation.

The circumstance that it is, for any several reasons, reasonable to consider convection only in a spherical shell, ignoring the central region, is another distinctive feature of models of convection and dynamo in spherical bodies. For geodynamo models, this is related to the fact that in certain models it is assumed that the solar magnetic field is generated in the $0.7 \leq r \leq 1$ radial layer (unity corresponds the dimension of the Sun) [Hollerbach and Rüdiger, 2004]. For planets (and the

Earth), the pressure in the central part is often so high that the matter is in the solid state in spite of high temperatures. Thus, the Earth's liquid core is the $0.35 \leq r \leq 1$ layer in units of the liquid core radius. On the one hand, the transition to the spherical layer can result in several simplifications: e.g., for the Sun, a small layer thickness forms the basis for the introduction of a small parameter and the development of an asymptotic analysis [Parker, 1979]. On the other hand, a visual analysis of convection in a spherical layer at small Rossby numbers (characterizing the ratio of the characteristic velocity to the daily rotation velocity) indicates that convection in the region above (below) the inner core and outside this region has different properties [Jones, 2000; Simitsev, 2004], which was repeatedly discussed in the literature. The separation of these regions is related to the so-called Taylor cylinder (TC), the axis of which coincides with the axis of rotation and the radius is equal to the inner core radius. In the presence of friction at the core boundaries, TC coincides with the Stewartson layers. However, the division into two different regions remains even when nonviscous boundary conditions are used. Increased interest to this problem is also related to the fact that geomagnetic activity at the intersection of TC with the Earth's surface ($\theta = 20.5^\circ$ is the angle counted off from the axis of rotation) is increased according to the geomagnetic observations [Olson, 2007].

Below we consider how convection can first originate outside TC and then be transferred into TC, depending on the amplitude of thermal sources. Helicity and differential rotation behave differently in these regions. These characteristics are of prime importance for understanding the problems of convection and dynamo in planets. Using a number of convection modes (typical of the geodynamo) in a spherical layer as an example, we indicate how these characteristics of flow change with increasing Rayleigh numbers.

2. CONVECTION EQUATIONS

We consider the convection equations for an incompressible fluid ($\nabla \cdot \mathbf{V} = 0$) in a spherical layer ($r_i \leq r \leq r_0$) rotating about the z axis at an angular velocity Ω , where (r, θ, φ) — is the spherical coordinate system [Jones, 2000]. We introduce the following units for velocity \mathbf{V} , time t , and pressure P — κ/L , L^2/κ , and $\rho\kappa^2/L^2$, respectively (here L is the unit of length, κ is the molecular thermal conductivity, and ρ is the matter density):

$$\begin{aligned} & EPr^{-1} \left[\frac{\partial \mathbf{V}}{\partial t} + (\mathbf{V} \cdot \nabla) \mathbf{V} \right] \\ &= -\nabla P - \mathbf{1}_z \times \mathbf{V} + Ra Tr \mathbf{1}_r + E \Delta \mathbf{V} \quad (1) \\ & \frac{\partial T}{\partial t} + (\mathbf{V} \cdot \nabla)(T + T_0) = \Delta T. \end{aligned}$$

The dimensionless Prandtl, Ekman, and modified Rayleigh numbers were specified as $Pr = \frac{\nu}{\kappa}$, $E = \frac{\nu}{2\Omega L^2}$, and $Ra = \frac{\alpha g_0 \delta T L}{2\Omega \kappa}$, where ν is the coefficient of kinematic viscosity, α is the coefficient of volumetric expansion, g_0 is the gravity acceleration, and δT is the unit of a temperature (T) disturbance relative to the equilibrium profile T_0 . We introduce the modified Rossby number, determined from the diffusion velocity, as $Ro = EPr^{-1}$.

Problem (1) has the boundary conditions at $r = r_i$, r_0 . Zero boundary conditions are used for temperature (T) disturbances, which (together with the T_0 profile specified above) corresponds to the fixed values of the total temperature $T_0 + T$: (1, 0). The condition of impenetrability $V_r = 0$ is accepted for the velocity field. The nonviscous boundary conditions are used for the velocity tangential components V_θ and V_φ (for more detail, see discussion about the boundary conditions for the geodynamo problems in [Reshetnyak, 2006]).

The control volume method [Patankar, 1980; Hejda and Reshetnyak, 2004] was used to numerically solve set (1); the equations were solved in terms of physical derivatives on shifted grids ($125 \times 125 \times 125$). The algorithm was adapted for multiprocessor computers [Reshetnyak and Steffen, 2005] using MPI. In the calculations we used $n = N_\theta \times N_\varphi + 2$ processors, where $N_\theta = N_\varphi = 12$ is the number of processors in the meridional (θ) and azimuthal (φ) directions.

3. TWO CONVECTION REGIONS

Below we consider three convection regimes

$$R1: Ra = 1 \times 10^2, \quad Pr = 1, \quad E = 10^{-4}, \quad Re \sim 40;$$

$$R2: Ra = 5 \times 10^2, \quad Pr = 1, \quad E = 10^{-4}, \quad Re \sim 300;$$

$$R3: Ra = 5 \times 10^3, \quad Pr = 1, \quad E = 10^{-4}, \quad Re \sim 2000,$$

with different amplitudes of thermal sources.

For the first regime ($R1$), the Ra value is close to its threshold value. For this range of parameters, convection appears outside the TC region and represents cyclones and anticyclones (CA) located along TC near its boundary. This type of convection is characterized by a high degree of geostrophy: if we accept that the characteristic wavenumber for cyclones is $m_c \sim 0.2E^{-1/3} = 4$ (see Fig. 1), the ratio of the nonlinear term amplitude to the Coriolis force will be $G_{R1} = ERe m_c \approx 0.016$. The regime close to rigid corotation at an angular velocity of $\omega < 0$, opposite to the direction of the planet's daily rotation Ω , is observed within TC: $\zeta = \omega\Omega < 0$ (Fig. 2). Convective heat exchange within a cylinder is absent ($Nu = 1$), Fig. 3. The maximal heat loss is reached outside TC at the equator (Fig. 4). A fluid is the warmest in the same region. Helicity $\chi = \langle \mathbf{V} \cdot \nabla \times \mathbf{V} \rangle_{\varphi, t}$, averaged over the azimuthal coordinate and time (Fig. 1), usually originates (for more detail, see [Reshetnyak, 2006]). The χ sign changes in the equatorial plane ($z = 0$). So strong difference between two regions within and outside TC is related to the fact that the energy of thermal sources cannot generate cyclonic convection within TC, where a fluid near the upper boundary should move perpendicularly to the axis (rather than at an angle, as is observed outside TC), owing to the geometry of the boundary. In this case the Coriolis force is more effective than outside TC, the flow scale decreases, and dissipation increases.

For $R2$ $G_{R2} \approx 0.1$ and is locally close to unity (i.e., the transient regime from geostrophic convection to the regime of inertial waves is observed); the energy of sources can already generate convection within TC. It is interesting that rotation (ω) in the opposite directions (which reverses along z in either hemisphere) appears in TC, and helicity χ changes its sign here. The angular velocity profiles $\omega(r)$ are still close to $R1$ (Fig. 2), but changes in the temperature (Fig. 4) and heat loss (Fig. 3) distributions are observed: the temperature in TC reaches that in the outer region.

We now estimate the differential rotation amplitude as $\mathcal{G} = s \frac{\partial \omega}{\partial s}$, where s is the distance to the z axis.

For the Northern Hemisphere, $\mathcal{G} > 0$ immediately above a core in TC, and $\mathcal{G} < 0$ at the upper boundary (Fig. 5). The accepted order of magnitude of the α effect amplitude is usually $\alpha = -\tau\chi/3 \lesssim \nu$, where $\tau = l/v$ is the characteristic time of an l -scale vortex rotation at velocity v . We introduce the magnetic field generation effectiveness, well-known in the $\alpha\omega$ dynamo theory: the so-called dynamo number $\mathcal{D} = \alpha\mathcal{G}$. It is evident that $\mathcal{D} < 0$ in the entire TC in the Northern Hemisphere; at the same time, for $R1$, $\mathcal{D} > 0$ in the Northern Hemisphere, and the generation maximum

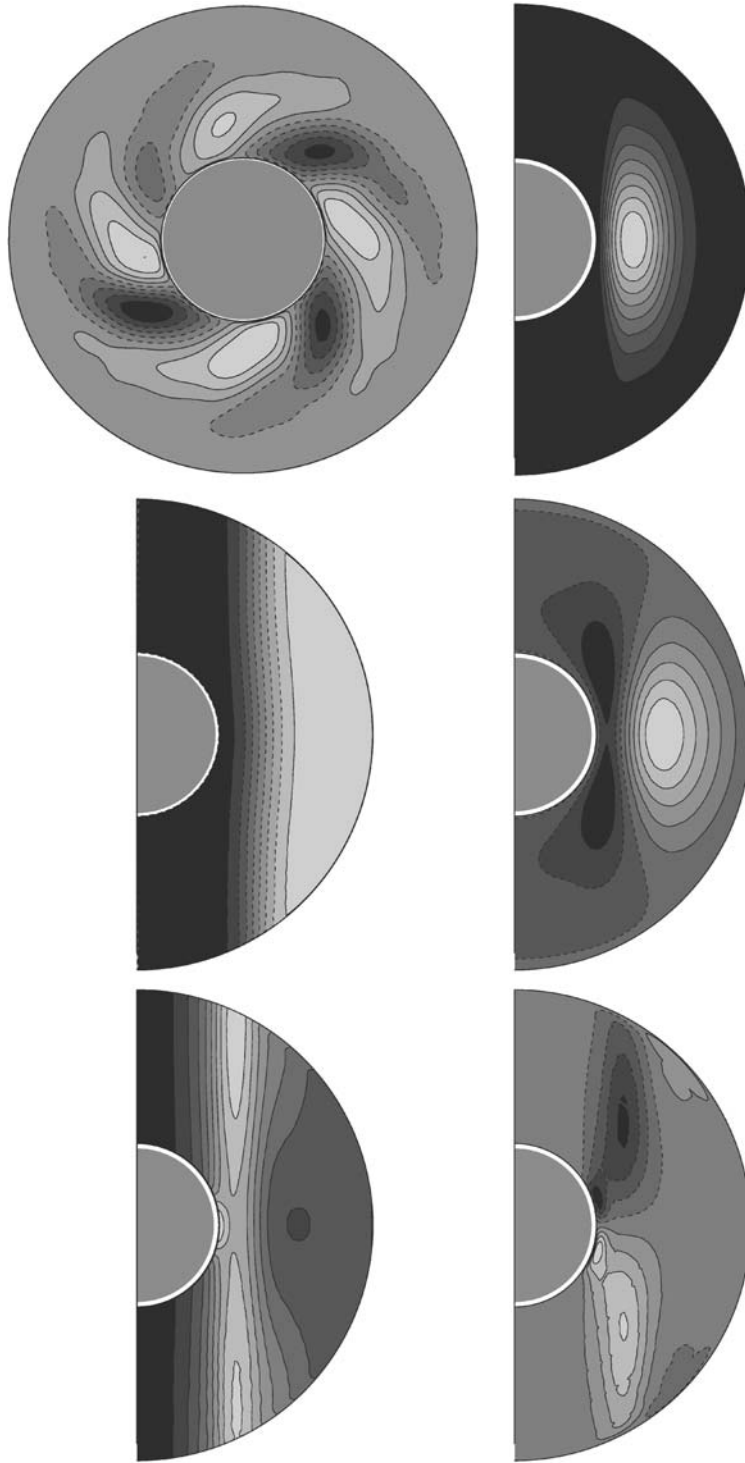


Fig. 1. Regime *R1*. The distribution of V_r ($-26.3, 17.4$), Nu ($1.0, 1.4$), ω ($-64.1, 17.1$), T ($-0.02, 0.04$), E_K ($0.0, 10^3$), and χ ($-4298, 4326$) (from the left to the right, from top to bottom). Dots correspond to the negative field values.

is outside TC. A change of the dynamo number (\mathcal{D}) sign is an important factor in the dynamo models and was repeatedly studied in the mean field models [Krause and Rädler, 1980; Jones, 1995]. Thus, long

intervals without inversions can appear at negative D [Reshetnyak and Pavlov, 2000].

For $R3$ $G_{R3} \approx 0.8$ and can locally be larger than unity. This is also the transient regime (as *R2*). A Taylor

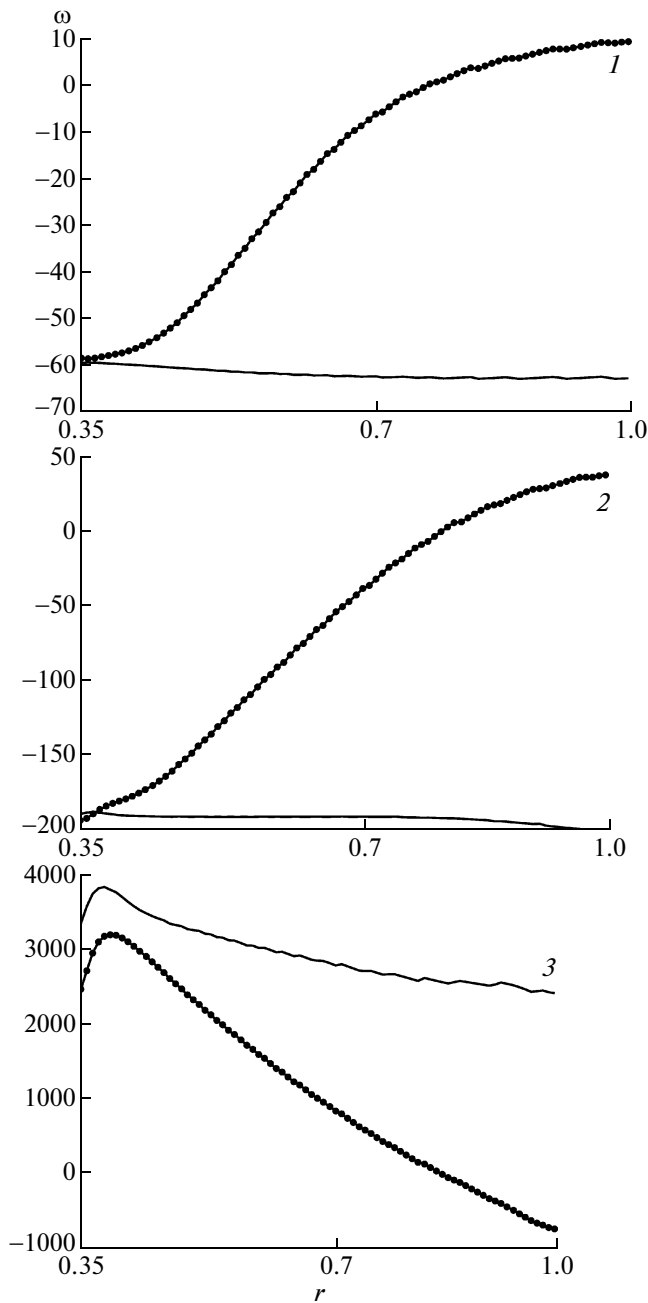


Fig. 2. The profiles of the rotation angular velocity (ω) along the radius for the R1 (1), R2 (2), and R3 (3) regimes within (a solid line) and outside (circles) TC.

cylinder, where heat exchange is mainly concentrated (Fig. 3), is the warmest (Fig. 4). Descending flows, cooling a fluid adjacent to the core, are located in the equatorial part (Fig. 6). In all three regimes, the equatorial part near the solid core remains to be the region with the highest energy. The behavior of the rotation curve $\omega(r)$ is reconstructed most substantially (Fig. 2). In TC $\omega > 0$, and \mathcal{G} is generally negative except quite small s . Outside TC ω is also positive, and $\mathcal{G} < 0$. Near the equator ω becomes negative. It is interesting that ω

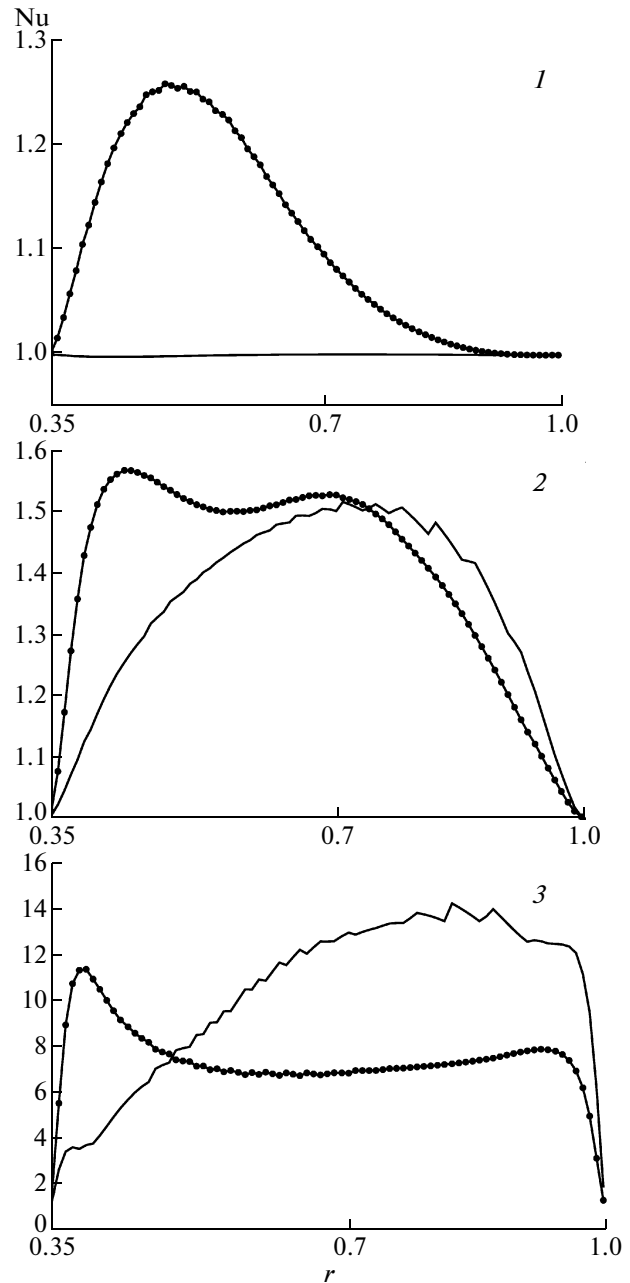


Fig. 3. The profiles of the Nusselt number (Nu) along the radius for the R1 (1), R2 (2), and R3 (3) regimes within (a solid line) and outside (circles) TC.

outside TC reversed its sign in all three cases. A strong azimuthal flow ($\omega > 0$), twisting also the adjacent regions outside TC, originates in TC. Only near the equator, ω becomes negative, and the amplitude of this flow remains several times as small as at high latitudes.

From the archeomagnetic data, it is known that the eastward drift of the nondipole field is observed together with the westward drift of the magnetic field. Two hypotheses exist concerning the drift origin. The first hypothesis is related to sliding of the frozen-in

magnetic field relative to the mantle due to the relative motion of the core and mantle fluid. The second hypothesis is related to the existence of waves caused by the magnetic–Archimedean–Coriolis forces (MAC waves) and is independent of mass transfer. Both westward and eastward waves are observed at the same latitudes, which is seemingly the argument for the MAC mechanism to a greater extent. However, we assume that the sliding mechanism can also exist since ω changes its sign along the radius outside TC in all three regimes.

For *R3*, the generation of χ decreased due to a decrease in the role of rotation and a decreased correlation between \mathbf{V} and $\text{curl}\mathbf{V}$ as a result of intensified motions. The centers of high χ are observed in TC and near the equator. The pattern becomes less regular.

We consider in more detail the dependence of the rotation angular velocity (ω) on the distance (s) to the axis (Fig. 7). Regimes *R1* and *R2* are close to each other and demonstrate an extremely extraordinary behavior from the standpoint of general concepts [Velikhov, 2005]: a rigid corotation within TC and near the equator and a monotonous increase in the region of CA existence. Convection specificity in the shell consists in that CA start generating Rossby waves, propagating in the azimuthal direction, with increasing Rayleigh numbers [Busse, 2002]. The wave direction depends on the type of the column height $h(s)$ function: decreasing (sphere) or increasing (paraboloid). For a sphere, the liquid core regions near the equator lead the rotation of the planet ($\zeta > 0$); at the same time, the regions near the pole rotate oppositely ($\zeta < 0$). For a paraboloid, the signs in the inequalities should be replaced by the opposite ones. It is interesting that curves 1 and 2 are in the unstable region near the poles and the equator according to the Rayleigh criterion of instability: $(\omega s^2)'_s < 0$. As was mentioned previously, convection near the poles is suppressed by the Coriolis force near solid boundaries. In the equatorial region, flows are arranged so that (for the Ra data) heat from the solid core is more effectively transferred near TC ($0.35 < s < 0.6$), inheriting the properties of the [Busse, 1970] linear solution, and the outer layers continue corotating rigidly.

Regime *R3* is substantially different: the outer layers start rotating oppositely to the planet's rotation ($\zeta < 0$), whereas the rotation maximum (corresponding to $\zeta > 0$) is observed within TC. The thermal wind

$(\frac{\partial V_\phi}{\partial z} \sim \text{Ra} \frac{\partial T}{\partial \theta})$ begins to penetrate from the region

outside TC into the inner region, resulting in that the entire TC starts rotating at $\zeta > 0$. Figure 6 clearly demonstrates that TC in the equatorial plane is replenished by approaching flows since a fluid is cold in this region. An increase in Ra results in a closer relation between two regions separated by TC. As we approach the upper boundary, ω decreases and remains positive (see

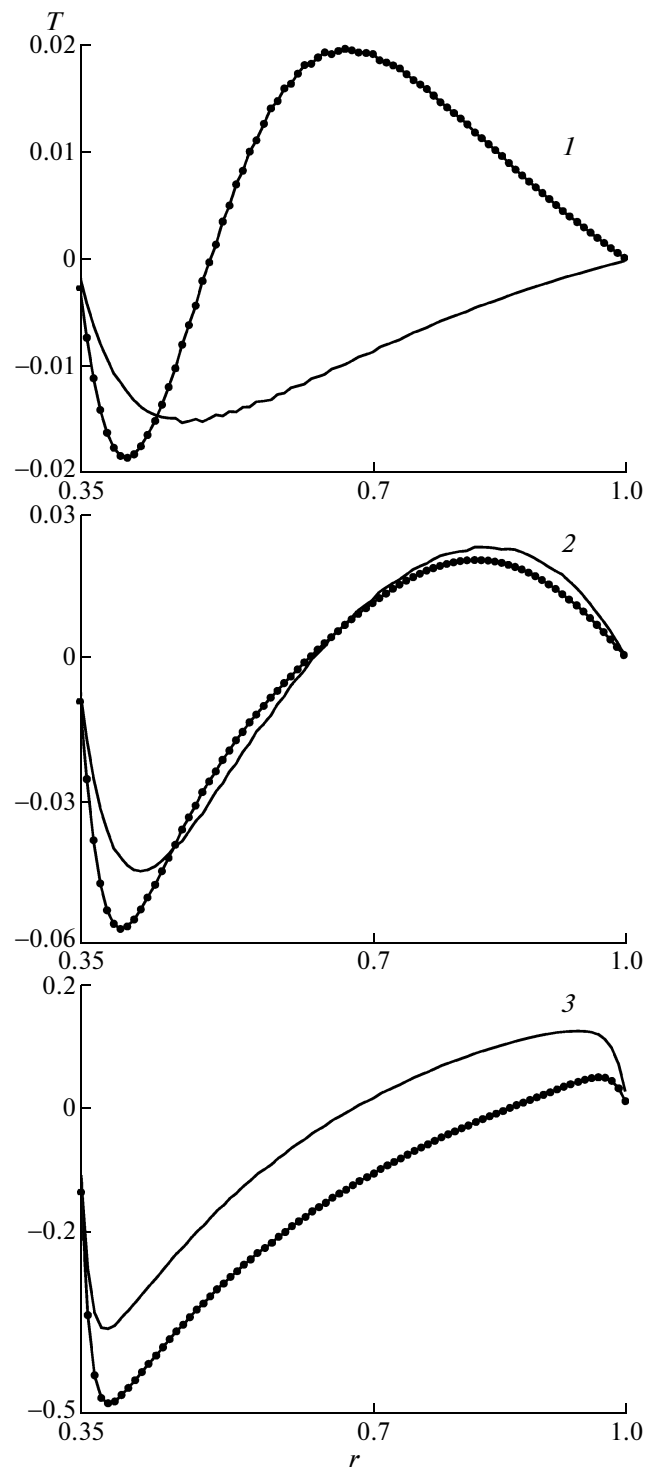


Fig. 4. The temperature (T) disturbances along the radius for the *R1* (1), *R2* (2), and *R3* (3) regimes within (a solid line) and outside (circles) TC.

in more detail an analysis for different Prandtl numbers in [Sreenivasan and Jones, 2006]). The presence of the temperature gradient in TC results in the linear profile for ω within TC. The regions within TC and

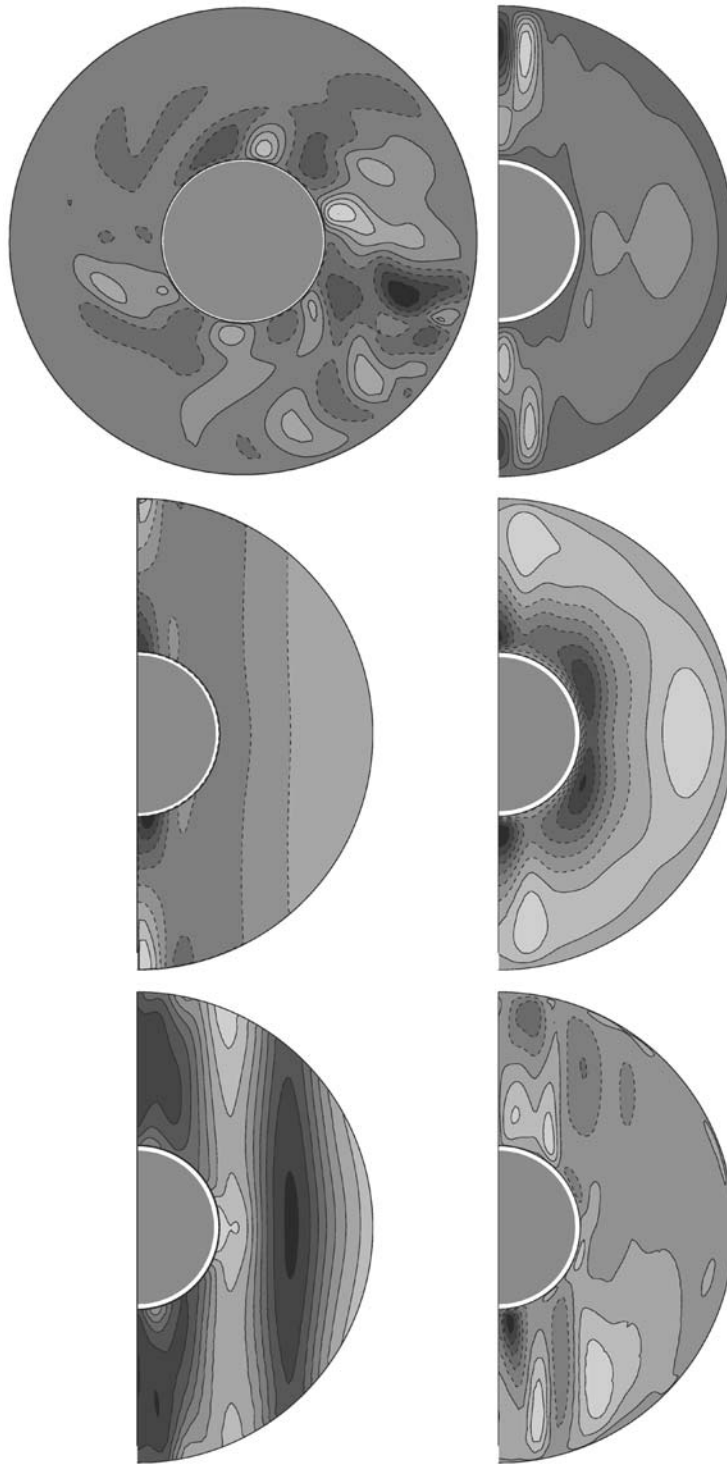


Fig. 5. Regime *R2*. The distribution of V_r ($-134, 136$), Nu ($-0.22, 3.0$), ω ($-780, 382$), T ($-0.08, 0.04$), E_K ($0.0, 1.6 \times 10^4$), χ ($-2 \times 10^5, 2 \times 10^5$) (from the left to the right, from top to bottom).

near the equator are unstable according to the Rayleigh criterion. It is interesting that the ω sign reversal in all three regimes is observed at $s \approx 0.6-0.7$ ($\theta \approx 35^\circ-45^\circ$). We also pay attention to the fact that the rotation

curve ω for the Sun has also the rotation minimum at the poles and the maximum near the equator, although this curve is less geostrophic [Hollerbach and Rüdiger, 2004].

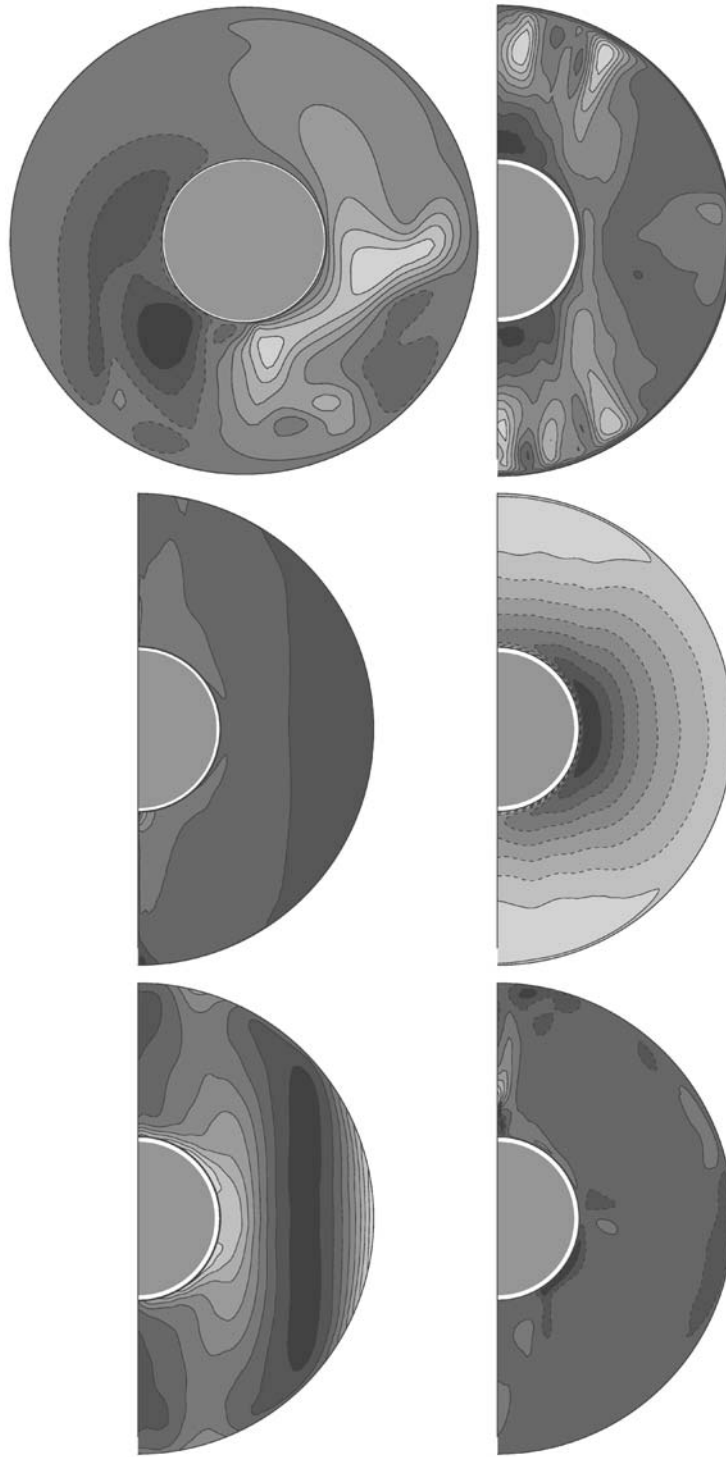


Fig. 6. Regime *R3*. The distribution of V_r ($-874, 1387$), Nu ($-7.3, 32.9$), ω ($-4909, 19490$), T ($-0.49, 0.14$), E_K ($0.0, 2.7 \times 10^6$), χ ($-3 \times 10^7, 3 \times 10^7$) (from the left to the right, from top to bottom).

4. FLOW RADIAL SYMMETRY

It is known that the topology of convective cells can be changed by reversing the $\beta = \frac{\partial v}{\partial T}$ sign [Getling,

1999]. It is customary to consider that a cell belongs to the *g* type ($\beta < 0$), if a matter (gases, gas) descends at the cell center. For fluids the situation is reverse: a substance ascends at the cell center, and $\beta > 0$. Such a cell

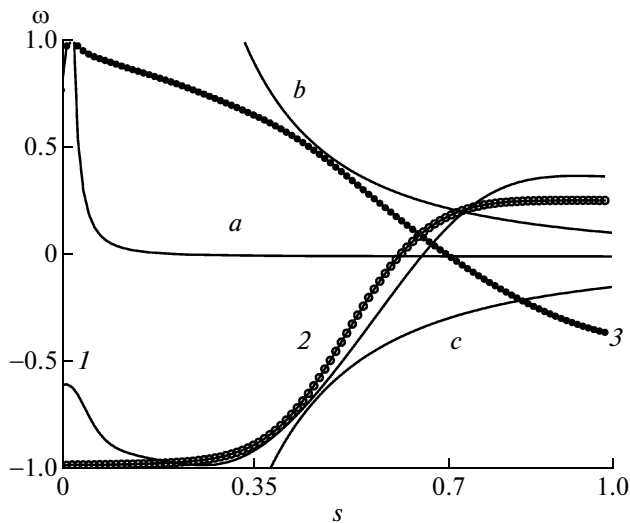


Fig. 7. The profiles of the rotation angular velocity $\omega(s)$ for the R1 (1), R2 (2), and R3 (3) regimes. Parabolas (a) and (b) are specified by the $f = A_i/s^2$ function, where $A_a = \omega_{R1}(0.01)$, $A_b = \omega_{R3}(0.46)$, and $A_c = -\omega_{R1}(0.46) \approx \omega_{R2}(0.46)$.

belongs to the l type (liquid). Assume that we have cells of the l type. In such a case, less deformations of a large-scale magnetic field are required to carry it downward than to push it onto the surface (in the first case, the Maxwellian tensions will be lower). It is said that ascending flows are topologically independent, whereas descending ones are related, as a result of which the term “magnetic field topological pumping” appeared [Drobyshevski and Yuferev, 1974; Vainshtein et al., 1980]. In due time this phenomenon made it possible to explain why a strong magnetic field is retained in the solar convective zone rather is pushed out of the generation zone onto the surface owing to a low density of the regions with strong magnetic fields. The asymmetry of convection cells is also known in the galactic dynamo, where hot mass ejections, forming l -type cells, are related to supernova explosions [Brandenburg et al., 1995].

The situation for the Earth’s liquid core does not formally correspond to the considered classifications since $\beta = 0$ is usually accepted for liquid iron. Even in going from the Boussinesq approximation to the so-called unelastic approximation, taking into account the effects of compressibility and the equation for entropy, one usually assumes that the medium molecular viscosity is constant. Below we consider how nonlinear effects can nevertheless result in breakdown of symmetry of ascending and descending flows in the problem in a spherical shell with constant coefficients at least for the case without rotation. I am grateful to V.P. Trubitsyn for the initiation of the studies in this direction.

According to a linear analysis, the structure of ascending and descending flows is identical in the case without rotation when the coefficients are constant at the generation threshold. With increasing amplitude of thermal sources, nonlinear effects originate, boundary layers are formed, and asymmetry can altogether appear. These effects are observed in the calculations for the mantle, where the $Pr \rightarrow \infty$ approximation is used. In this case a grid of descending cold flows originates on the surface, whereas approaching warm flows have the shape of plumes. At the lower warm boundary, the pattern is opposite: a grid of a superheated fluid originates, and a cold fluid has the shape of plumes. It is interesting that tessellation granules with dark edges are also observed on the Sun. These facts as well as the numerical experiments make it possible to state that the response slightly depends on the type of boundary conditions for the velocity at the boundary since the conditions of non-slippage and absence of viscous tensions are usually accepted for the mantle and gaseous bodies, respectively. Below we quantitatively estimate the originating asymmetry and the dependence of the effect on the Prandtl number.

Figure 8 presents the section near the lower and upper boundaries for small and large Prandtl numbers. For large Prandtl numbers, the above effect is clearly defined: the grids of warm and cold flows from below and above, respectively. For $Pr = 1$, such a difference is already absent. We estimate the areas of ascending (S_1) and descending (S_2) flows as a function of radius r (the $S_1(r)$ and $S_2(r)$ values are normalized so that $S_1 + S_2 = 1$ for any r), see Fig. 9. The $Pe = 1 \rightarrow 10$ transition is evident when the monotonically decreasing function R is transformed into the monotonically increasing function, Fig. 9(3). Figures 9(1) and 9(2) correspond to the appearance of “nails” and “mushrooms.” At small Prandtl numbers ($\nu < \kappa$), a flow has time to cool due to the effects of thermal conductivity and isotherms correspond to “nails” when approaching the upper boundary. For $\nu > \kappa$, isotherms at the upper boundary resemble caps (or a thermonuclear explosion). In this case a matter has been brought “too” rapidly, and a time is required for its cooling.

In spite of the fact that the phenomenon of warm and cold grids at the boundaries has long been known in the numerical experiments, it has not yet been explained rigorously. Assume that $Pr \gg 1$ (the scale of changes T is small). The originating fluctuations of T in the boundary layer at the lower boundary result in the appearance of a two-dimensional grid of ascending flows. At the same time, cold flows, which have a cylindrical shape and fall on the center of a convective cell, descend on the lower boundary. A cylindrical shape is optimal from the standpoint of a decrease in frictional forces. The opposite effect is observed at the upper boundary: a cold grid is formed. At $Pr \sim 1$, the scale of thermal fluctuations at the boundaries substantially increases (Fig. 8). A nail pointed upward is

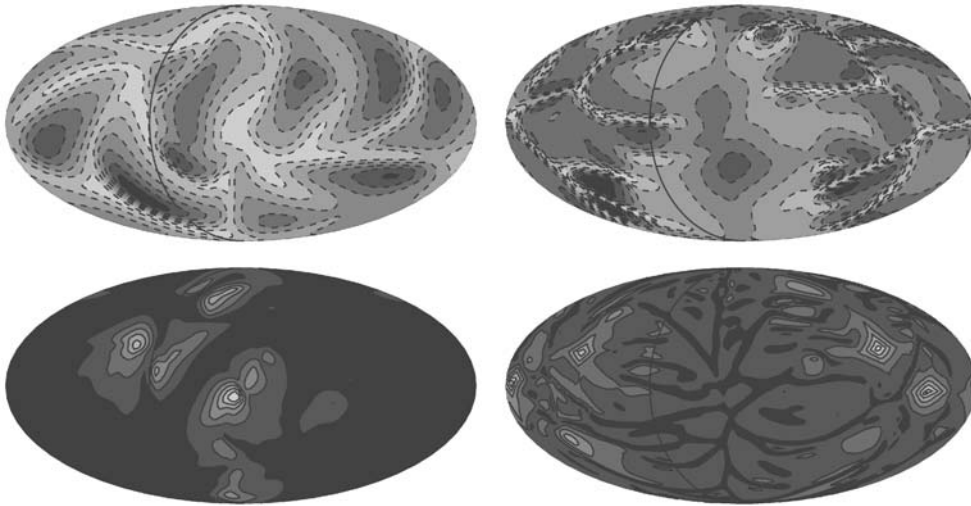


Fig. 8. The distribution of the temperature (T) disturbance for $r=0.36$ (the upper two figures) and $r=0.99$ (the lower two figures) for $\text{Pr} = 1$, $\text{Ra} = 10^7$, $E = 1$ (the left column) $(-0.22, 0.00)$, $(0.00, 0.27)$ and $\text{Pr} = 10^3$, $\text{Ra} = 10^8$, $E = 1$ (the right column) $(-0.30, -0.04)$, $(0.01, 0.22)$. The values in parentheses correspond to the range of field variations.

formed at the lower boundary (S_1 decreases). Nails of cold flows of these fluctuations pointed downward appear at the upper boundary.

Similar experiments for plane geometry at the early state of flow formation confirm the results for spherical geometry. However, one not always succeeds in obtaining considerable R variations on large time scales due to the formation of horizontal shafts, leading to the distortion of asymmetry in the main volume and to the $R \sim 1$ values.

The introduction of rotation is critical for this type of asymmetry (see Fig. 8): the deviation of R from unity is much smaller than in the case without rotation and already depends on the Rayleigh number. In this respect, it is interesting that another type of asymmetry exists [Sreenivasan and Davidson, 2008]: cyclones predominate over anticyclones when the Rossby numbers are about unity. This type of asymmetry is of little interest for the Earth's core (the Rossby number in the Earth's core is much smaller than unity); at the same time, this effect is worthy of consideration for the solar dynamo.

5. DISCUSSION

We consider how the results, achieved for the regimes with rotation, can be used to describe the processes in the Earth's core. It is known [Hunter and Riahi, 1975; Boubnov and Golitsyn, 1995] that the effect of rotation on thermal convection can be estimated based on the ratio of the Rayleigh ($\widehat{\text{Ra}} = \text{Ra}E^{-1}$) and Taylor ($\text{Ta} = E^{-2}$) numbers. These data were obtained for convection in a plane layer with heating from below but are also applicable to spherical geometry. Convection is possible at $\text{Ta} \ll W$ ($W = \widehat{\text{Ra}}^{3/2}$). At

$\widehat{\text{Ra}} \gg \text{Ta}$, the role of rotation is insignificant (*i*). At $\widehat{\text{Ra}} \ll \text{Ta} \ll H$ ($H = \widehat{\text{Ra}}^{4/3}$), rotation can lead to enhancement of a thermal flow (*ii*) under the conditions of non-slippage [Rossby, 1969]. The latter is related to the fact that the thermal boundary layer is "pressed" by the Ekman layer when Ta increases. For $H \ll \text{Ta} \ll W$, rotation results in weakening of a thermal flow and cessation of convection (*iii*). However, a thermal flow cannot increase for the *ii* regime, even if the viscous boundary conditions are taken into account, because the thickness of the Ekman layer in the liquid core is less than that of the thermal boundary layer (the molecular value of the Prandtl number is $\text{Pr} = 0.1$).

For the Earth's liquid core [Christensen and Aubert, 2006], $\widehat{\text{Ra}}_{\otimes} \sim 10^{23}$ and $\text{Ta}_{\otimes} = 4 \times 10^{28}$, so that $\text{Ta} < \widehat{\text{Ra}}^{4/3} = 4 \times 10^{30}$; i.e., the *ii* regime is observed. The presented estimates correspond to the case when Ra is larger than the critical value (Ra^{cr}) at the excitation profile by a factor of 5000. A more conservative estimate is $\text{Ra} \sim 500\text{Ra}^{\text{cr}}$ [Jones, 2000]. The $R1$ – $R3$ regimes considered above fall also in the range (*ii*): $\text{Ta}_{R1} = \text{Ta}_{R2} = \text{Ta}_{R3} = 10^8$: $\widehat{\text{Ra}}_{Ri} < \text{Ta}_{Ri} < H_{Ri}$, where $\text{Ra}_{R1} = 10^6$, $\widehat{\text{Ra}}_{R2} = 5 \times 10^6$, $\widehat{\text{Ra}}_{R3} = 5 \times 10^7$, $H_{R1} = 10^8$, $H_{R2} = 8 \times 10^8$, and $H_{R3} = 4 \times 10^{11}$.

Coincidence in the Nusselt number is another important parameter. For the Earth, $N_{\otimes} \sim 10^6$ [Christensen and Aubert, 2006], which cannot certainly be reached in the scope of laminar models. At the same time, $\text{Nu}(r)$ becomes stable and boundary layers are formed with increasing Ra (Fig. 3), which also makes it possible to hope that the results of the $R2$ – $R3$

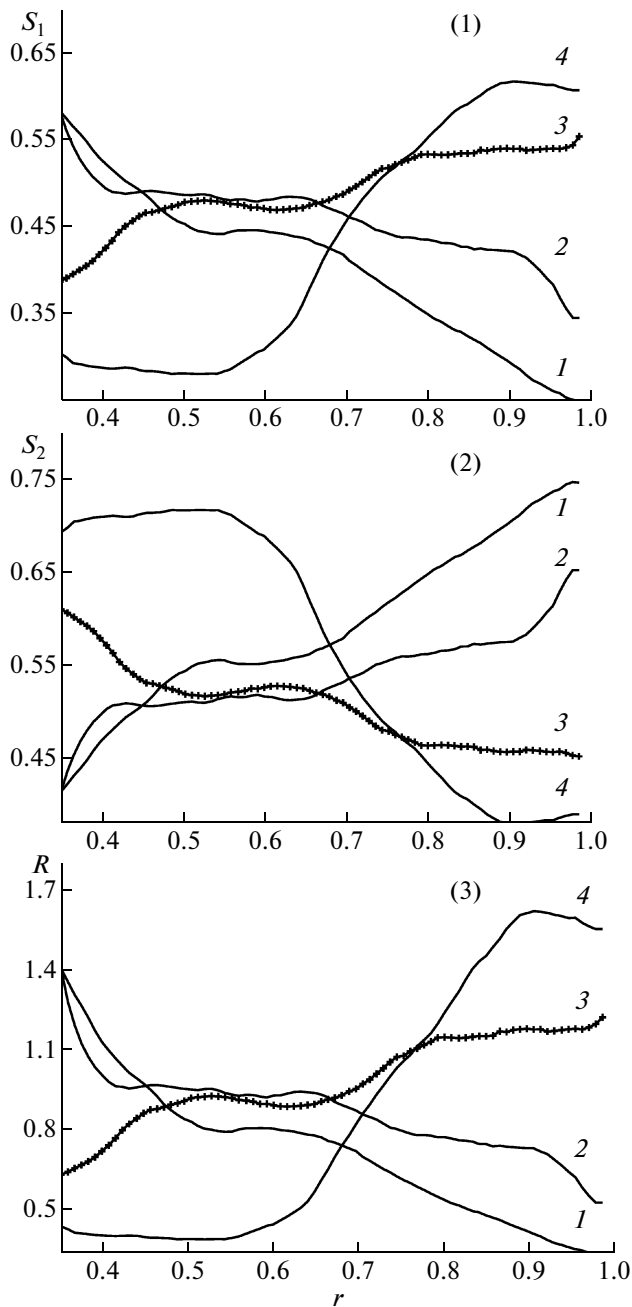


Fig. 9. (1) The contribution of the ascending flow area ($V_r > 0$) S_1 for the thermal convection model as a function of radius r (during insignificant rotation, $E = 1$). (1) $Pr = 1$, $Ra = 10^6$, and $Re \sim 200$; (2) $Pr = 0.1$, $Ra = 10^7$, and $Re \sim 3100$; (3) $Pr = 10$, $Ra = 10^7$, and $Re \sim 83.4$; and (4) $Pr = 100$, $Ra = 10^7$, and $Re \sim 10$. (2) The same regimes for the area of descending flows ($V_r < 0$) S_2 as a function of radius r (during insignificant rotation, $E = 1$). (3) The $R(r) = S_1/S_2$ ratio.

regimes can be extrapolated for the Earth's conditions. However, the $R3$ regime is more suitable concerning the supercriticality of thermal sources (Ra values). Taking into account the fact that a large-scale spirality

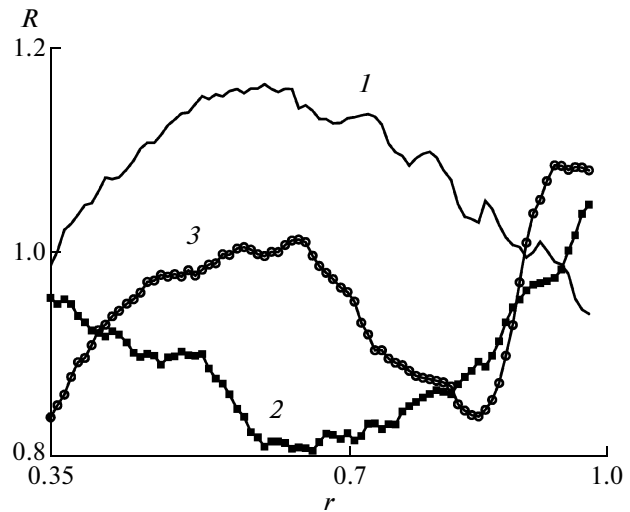


Fig. 10. The $R(r) = S_1/S_2$ ratio for the $R1$ (1), $R2$ (2), and $R3$ (3) regimes.

of this regime is not observed, we can consider it in the class of a large-scale dynamo, where the role of the α effect is insignificant. At present, the classification of the Earth's dynamo in terms of mean-field models is the problem to be solved [Sokolov, 2004]. The pioneer models by Braginsky (specifically, the Z model [Braginsky, 1978]) belonged to the type of $\alpha\omega$ models. In the scope of these models, toroidal magnetic fields, hidden from us by the nonconductive mantle layer, are substantially larger than poloidal fields. The following three-dimensional calculations [Jones, 2000] indicated that the ratio of these fields (\mathcal{Y}) is close to unity, which was an argument for $\alpha^2\omega$ models, where toroidal and poloidal fields are also comparable. On the other hand, the α effect is evidently zero and $\mathcal{Y} \sim 1$ in going to the regime without rotation, where the magnetic field can also be generated by large-scale flows. The calculations indicate that the role of spirality for $R1$ and $R2$ regimes decreases with increasing Ra . Therefore, it seems interesting to subsequently consider the limitations imposed by the magnetic field generation (a change in the magnetic spectrum at an increase in Ra) and to estimate the necessity of using the small-scale mechanism to explain the observed magnetic field. Note that pumping of the magnetic field from small scales to large ones must be accompanied the inverse process of energy transfer from large scales to small ones at least because dissipation on large scales is insignificant. The latter is rarely discussed in the mean-field dynamo models, where it is usually accepted that velocity field is specified, and the transition to the quasistationary state is performed through the suppression of the α effect, which is far from the only possible explanation of the existence of such a state. This can be demonstrated by the results achieved in [Reshetnyak and Hejda, 2008], where the magnetic energy fluxes in the wave space were esti-

mated for a rotating layer heated from below. It turns out that the fluxes are extremely low for the scales larger than $LE^{1/3}$: more exactly, the energy flux (from small scales to large ones) of the $((\mathbf{B} \cdot \nabla)\mathbf{V})$ term, including the α and ω effects, is neutralized by the convective flow $(\mathbf{V} \cdot \nabla)\mathbf{B}$ from large scales to small ones to a high degree of accuracy. In total, these two terms give zero flux. In other words, an inverse effect of the magnetic field is reduced to “washout” of the magnetic field into the region of small scales and the following dissipation rather than to the suppression of the α effect.

REFERENCES

- B. M. Boubnov and G. S. Golitsyn, *Convection in Rotating Fluids* (Kluwer, London, 1995).
- S. I. Braginskii, “An Almost Axially Symmetric Model of the Earth’s Geomagnetic Dynamo,” *Geomagn. Aeron.* **18** (2), 340–351 (1978).
- A. Brandenburg, D. Moss, and A. Shukurov, “Galactic Fountains as Magnetic Pumps,” *Mon. Not. R. Soc.* **276**, 651–662 (1995).
- F. H. Busse, “Convective Flows in Rapidly Rotating Spheres and Their Dynamo Action,” *Phys. Fluids* **14** (14), 1301–1314 (2002).
- F. H. Busse, “Thermal Instabilities in Rapidly Rotating Systems,” *J. Fluid Mech.* **44**, 441–460 (1970).
- S. Chandrasekhar, *Hydrodynamics and Hydromagnetic Stability* (Dover Publ., New York, 1981).
- U. R. Christensen and J. Aubert, “Scaling Properties of Convection-Driven Dynamos in Rotating Spherical Shells and Applications to Planetary Magnetic Fields,” *Geophys. J. Int.* **166**, 97–114 (2006).
- Core Dynamics in Treatise on Geophysics, Vol. 8, Ed. by P. Olson (2007).
- E. M. Drobyshevski and V. S. Yuferev, “Topological Pumping of Magnetic Flux Three-Dimensional Convection,” *J. Fluid Mech.* **65** Part 1, 33–44 (1974).
- A. V. Getling, *Rayleigh–Benard Convection* (Editorial URSS, Moscow, 1999) [in Russian].
- P. Hejda and M. Reshetnyak, “Control Volume Method for the Thermal Convection Problem in a Rotating Spherical Shell: Test on the Benchmark Solution,” *Stud. Geophys. Geod.* **48**, 741–746 (2004).
- R. Hollerbach and G. Rüdiger, *The Magnetic Universe* (Wiley, Weinheim, 2004).
- C. Hunter and N. Riagi, “Nonlinear Convection in a Rotating Fluid,” *J. Fluid Mech.* **72**, 433–454 (1975).
- C. A. Jones, “Convection-Driven Geodynamo Models,” *Philos. Trans. R. Soc. (London)*, A **358**, 873–897 (2000).
- C. A. Jones, “Dynamo Models and a Taylor Restriction,” in *Space Magnetohydrodynamics*, Ed. by E. Priest and A. Hood (Mir, Moscow, 1995).
- F. Krauze and K.-H. Rädler, *Mean-Field Magnetohydrodynamics and Dynamo Theory* (Pergamon, Oxford, 1980; Mir, Moscow, 1984).
- E. N. Parker, *Cosmical Magnetic Fields: Their Origin and Their Activity* (Clarendon Press, Oxford, 1979; Mir, Moscow, 1982).
- S. V. Patankar, *Numerical Heat Transfer a Fluid Flow* (Taylor Francis, New York, 1980).
- J. Pedlosky, *Geophysical Fluid Dynamics* (Springer, New York, 1987).
- M. Reshetnyak and B. Steffen, <http://www.srcc.msu.su/num-meth/English/index.html>.
- M. Reshetnyak and P. Hejda, “Direct and Inverse Cascades in the Geodynamo,” *Nonlin. Proc. Geophys.* **15**, 873–880 (2008).
- M. Yu. Reshetnyak and V. Yu. Pavlov, “On Different Regimes of the Geomagnetic Field Generation for the Last 165 MA,” *Dokl. Akad. Nauk* **372**, 683–686 (2000).
- M. Yu. Reshetnyak, “Hydromagnetic Spirality in the Geodynamo Models of the Boussinesq Type,” *Fiz. Zemli*, No. 6, 3–13 (2006).
- H. T. Rossby, “A Study of Benard Convection with and Without Rotation,” *J. Fluid Mech.* **36**, 309–337 (1969).
- R. Simitev, PhD Thesis (University of Bayreuth, Bayreuth, 2004). <http://www.phy.uni-bayreuth.de/theo/tp4/members/simitev.html>.
- D. D. Sokoloff, “Geodynamo and Models of Geomagnetic Field Generation: A Review,” *Geomagn. Aeron.* **44** (5), 579–589 (2004) [*Geomagn. Aeron.* **44** (5), 533–542 (2004)].
- B. Sreenivasan and K. Jones, “Azimuthal Winds, Convection and Dynamo Action in the Polar Regions of Planetary Cores,” *Geophys. Astrophys. Fluid Dyn.* **100** (4–5), 319–339 (2006).
- B. Sreenivasan and P. A. Davidson, “On the Formation of Cyclones and Anticyclones in a Rotating Fluid,” *Phys. Fluids* **20**, 085104-1–085104-11 (2008).
- S. I. Vainshtein, Ya. B. Zel’dovich, and A. A. Ruzmaikin, *Turbulent Dynamo in Astrophysics* (Nauka, Moscow, 1980) [in Russian].
- E. P. Velikhov, “Magnetic Hydrodynamics,” *Pis’ma Zh. Eksp. Teor. Fiz.* **82** (11), 785–790 (2005).